Atomic redistribution of implanted Fe and associated defects around moving SiO 2 /Si interfaces

Anthony de Luca, Nelly Burle, Alain Portavoce, Catherine Grosjean, Stéphane Morata, Michael Texier

pss-Header will be provided by the publisher

Atomic redistribution of implanted Fe and associated defects around moving SiO_2/Si interfaces

Anthony De Luca[1], Nelly Burle[1]*, Alain Portavoce[1], Catherine Grosjean[2], Stéphane Morata[3], Michaël Texier[1]

[1] Aix Marseille Université, CNRS, IM2NP UMR 7334, bd Escadrille Normandie Niémen F-13397 Marseille, France
[2] ST Microelectronics, ZI Peynier Rousset F-13790 Peynier, France
[3] Ion Beam Services, ZI Peynier Rousset F-13790 Peynier, France

Received ZZZ, revised ZZZ, accepted ZZZ
Published online ZZZ (Dates will be provided by the publisher.)

Keywords : TEM, diffusion, contamination, oxide.

The behaviour of Fe atoms at the Si/SiO_2 interface, as a modelisation of an involuntary Fe contamination before or during the oxidation process has been studied in Fe-implanted wafers. As-implanted and oxidized wafers were characterized by SIMS, APT, HR-TEM and STEM-HAADF. Successive steps of Fe segregation, iron-silicides precipitation and dissolution were identified. As expected for such a temperature range, the iron-silicide precipitates adopt the $FeSi_2$ structure. Fe enriched phases were also identified in an advanced step of precipitation. Dynamic mechanisms are proposed, taking into account the competitive oxidizing of precipitates and silicon matrix, to understand the different steps and precipitation phases observed in the samples during the non-equilibrium conditions due to the oxide layer growth. The correlation between the formation of characteristic pyramidal defects at the SiO_2/Si interface and the presence of the Fe-rich precipitates is explained.

1 Introduction Silicon oxide remains the main gate oxide used in C-MOS technology. It still plays a key role in the advanced MOSFET technology as constituting a thin transition layer between the Si substrate and the high-k gate oxide layer [1]. However, metallic impurities in silicon, even for low contamination levels, may affect hugely the reliability of the component by creating electric defects in the active region as well as by disturbing the quality of the interface SiO_2/Si.

Iron is one of the most deleterious metallic contaminants in silicon; various steps of the process can lead to Fe contamination *via* different sources (polishing slurries, impurities in quartz tubes material, SiC boats, furnaces liners) [2], and because its high diffusivity [3] and capacity to act as donor [4] it is known to strongly degrade the device performances.

Fe contamination may affect the SiO_2/Si interface integrity as it has been shown in various studies. For example, Honda *et al*., showed that α-$FeSi_2$ precipitates can nucleate at the SiO_2-Si interface, which is responsible for the increase of leakage currents and leads to dielectric breakdown in MOS capacitors [5]. SIMS measurements performed on Fe-contaminated, dry-oxidized Si wafers also evidenced iron atoms accumulation at the SiO_2/Si interface while a part of the iron atoms is trapped in the oxide layer [6]. Sadamitsu *et al*. identified the precipitation of the cubic phase FeSi at the Si/SiO_2 interface and identified inclusions in the oxide as probably being Fe_3O_4 and γ-Fe_2SiO_4 precipitates [7]. Pyramidal defects and β-$FeSi_2$ precipitates have been observed , with the same density, at the SiO_2/Si interface in surface Fe-contaminated Si wafers [8]. These authors suggested that the injection of excess self-interstitial Si atoms by $FeSi_2$ precipitation would enhanced the formation of such pyramids. Anyway, the alteration of electrical characteristics of devices would be due not only to the Fe-induced levels in the gap, but also to the reduction of the grid oxide thickness [6]. It must be noticed that the size of the observed precipitates does not change with the contamination level and remains close to 10 nm in diameter. Similar pyramidal defects and precipitates were not observed in bulk-contaminated samples.

The aim of this work is to evidence the links between the two main defects in iron-contaminated wafers: precipitates and pyramidal defects, and to justify this correlation.

2 Materials and methods Fe implantation has been performed in P doped (2-20 Ω·cm) (001) Si wafers (extraction voltage of 65 kV, fluence of 1.0×10^{15} atoms·cm^{-2}). The incidence angle of 7 ° from the Si(001) surface allowed reducing the channelling effect [9, 10].

SIMS measurements were performed in as-implanted and oxidised samples until 500nm in depth. Fe-implantation profiles were also simulated by Stopping and Range of Ions in Matter (SRIM) calculations [11], taking into account the possible mixing artefact [12] , and by Atomic Probe Tomography (APT). These various techniques gave well correlated results; the concentration profiles follow a gaussian distribution centred on a 55 nm-average implantation depth.

Oxidation of the implanted wafers was carried out by thermal annealing in oxygen atmosphere at 900 °C or 1100 °C for various durations. For this, the wafers were first introduced in a furnace at 800 °C under N_2 flux. Afterward, the wafers were maintained under $(N_2)_{90\%}$ $+(O_2)_{10\%}$ flux to avoid undesired nitriding of the surface while the temperature was increased using a ramp of 5 °C·min^{-1} until the annealing temperature (900 °C or 1100 °C) was reached. After being annealed under O_2 flux, the oxidized wafers were then cooled down to the room temperature under N_2 atmosphere at 5 °C·min^{-1}. Oxide layer thicknesses were determined using ellipsometry measurements.

Samples for transmission electron microscopy (TEM) and scanning transmission electron microscopy (STEM) analyses were prepared by focused ion beam (FIB) micromachining using a FEI Helios 600 Nanolab microscope equipped with a Ga^+ ion source.

TEM and STEM analyses were performed using a FEI Titan 80-300 C_s-corrected microscope operating at 300 kV and equipped with annular HAADF-STEM detector. For both optimizing spatial resolution and reducing spatial delocalisation, spherical aberration C_s was adjusted to -7 µm for TEM imaging.

3 Results and discussion

2.1 Fe implantation and precipitation SIMS measurements and APT analyses revealed that the initial Fe distribution follows a gaussian profile with a maximum concentration at the depth of 55 nm. In as-implanted samples, the presence of a superficial amorphous layer (thickness: 92±5 nm) was evidenced by TEM imaging.

However, the recrystalisation of this layer was ever complete in the sample annealed at 900 °C during 5 min, which is not surprising since the recrystallisation rate is estimated to at least 1800 nm·mn^{-1} at 800°C [14] so the whole 92 nm would be cured in less than 30 s . This fast recrystalisation leads to the formation of numerous end-of-range (EOR) defects [15] in the area corresponding to the initial interface between amorphous and crystalline silicon. However, no Fe segregation is evidenced on these defects, in contrast with the observation of Fe-decorated extended defects already reported in various studies [16--19]. In spite of the very short duration of the thermal annealing performed on this sample, *post mortem* TEM analysis also reveals the presence of precipitates at the SiO_2/Si interface. A rough estimation of 3×10^8 precipitates per surface square centimetre is found. The observed precipitates exhibit facetted shapes, with facets parallel to the {114} and {111} atomic planes of the Si substrate. These precipitates reach in few cases a few tens of nanometres in diameter. It must be noticed that they are systematically totally included in the silicon substrate.

On the contrary, the precipitates observed in samples annealed for a longer time (*i.e.* 3h and 10h) usually straddle the interface between the substrate and the oxide layer. In that case, although the precipitates' density and size (between 20 nm and 50 nm) remain similar to the ones of the precipitates observed in the sample annealed during 5 min, their shape is slightly different. In particular, the part of the precipitates embedded in the oxide layer is rounded, that is in sharp contrast with the other part, faceted, contained in the silicon substrate (figure 1). This morphological change suggests that the precipitates were partially oxidized during the oxidation process of the silicon, leading to a vanishing of the faceting imposed by the symmetry of the surrounding crystalline matrix when included in the silicon substrate, to the benefits of a more energetically favourable spherical shape in the amorphous oxide layer. The analysis of the Fourier transform of the HRTEM images systematically confirms that the structure of these precipitates coincides with the β-$FeSi_2$ silicide.

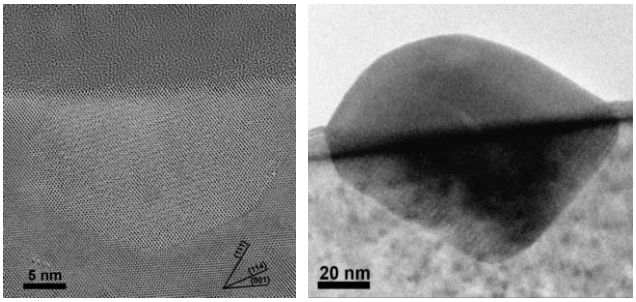

Figure 1 Precipitates observed in Fe-implanted silicon substrate (fluence: 1.0×10^{15} cm^{-2}) and dry-oxidized at 900 °C during a) 5 min (left) and b) 10 hours (right).

2.2 Pyramidal defects at SiO_2/Si interfaces and correlation with precipitates Numerous pyramidal defects, identified from HRTEM imaging as crystalline silicon, were systematically observed at the SiO_2/Si interface in all samples. Their density and size are roughly about 2×10^8 cm^{-2}, 10 nm × 30 nm in 900 °C samples, about 3×10^7 cm^{-2}, 10-30 nm × 60 nm in 1100 °C samples (estimated from TEM observations).

Moreover, spherical β-$FeSi_2$ precipitates were frequently observed at the top of pyramids (figure 2), that is supporting the hypothesis of a correlation between the presence of the precipitates and the formation of the pyramids. In the case of softer pyramids, smaller FeSi precipitates have also been identified, whereas their small size can

avoid them to be systematically detected. Finally, STEM-HAADF imaging revealed the presence of small Fe-rich clusters at the vicinity of pyramids in the oxide layer.

Considering the respective oxidation rates of silicon and iron-silicide precipitates, a faster oxidation rate of the β-$FeSi_2$ precipitates in comparison with silicon would systematically lead to the observation of precipitates totally embedded in the silicon layer. On the contrary, the observation of some of them partially or totally included in the oxide layer necessarily implies that bulk silicon is faster to oxidise than $FeSi_2$ precipitates. Thus, natural explanation of figure 2 is that the precipitate hinders the oxydation of silicon.

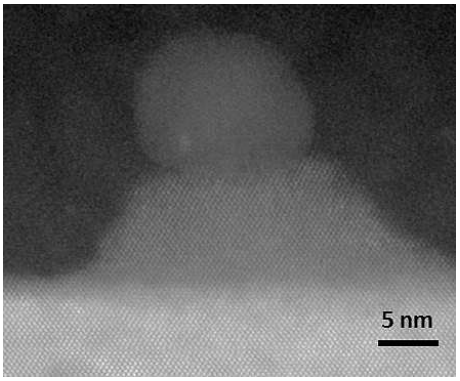

Figure 2 Example of pyramidal defect observed at the SiO_2/Si interface in oxidized silicon substrates previously implanted with Fe atoms, observed by HAADF-STEM imaging. Annealing conditions are 1100 °C, 12 min but similar configurations are observed in the others annealing conditions (except 900 °C, 5 min). The precipitate composition is $FeSi_2$.

The advance of the SiO_2/Si interface being locally masked by the presence of a precipitate, a pyramid is formed below. Nevertheless, the lateral sides of pyramids are also oxidised, which progressively leads to the inclusion of the precipitate in the growing oxide layer. As far as the precipitate is totally included in the oxide, the pyramid is progressively consumed in the same time the interface is moving forwards. The shape evolution of pyramids would probably follow the sketch illustrated in figure 3.

Some pyramidal defects are also observed whereas no precipitate is visible (figure 3). It could be attributed to natural roughness of the layer, but the most probable explanation is that the thinning of the sample can be located out of the medium plane of the pyramid so that the sample surface would be crossing the basis of the pyramid without intersecting the precipitate.

2.3 Diffusion of chemical species inside the precipitates Two main observations give evidence of competition between the moving of interface and some diffusion mechanisms:

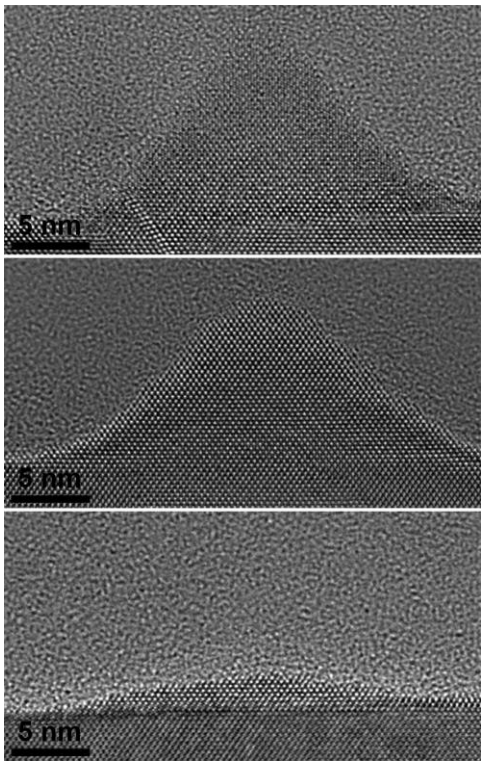

Figure 3 Various pyramidal defects observed at the SiO_2/Si interface in oxidized silicon substrates previously implanted with Fe atoms; Si pyramids are clearly coherent with the Si substrate. A stacking fault is visible within the pyramidal defect on the upper image.

a) SIMS measurements reveal that the maximum concentration of iron is always located at the interface, in good agreement with TEM observations in which big precipitates are consistently located in the vicinity of the SiO_2/Si interface whatever the oxidising time. So we can conclude that whereas the oxidation of Si is quicker than the oxidation of $FeSi_2$, the precipitates move with the interface. It implies both dissolution of the part of the precipitates included in the growing silicon oxide layer an the continuous growing of the $FeSi_2$ phase at its interface with the silicon substrate; this is possible only if Fe atoms diffuse towards the substrate, whereas Si in $FeSi_2$ is oxidized on the top part;

b) In some cases, some other phases with higher Fe contents have also been observed, corresponding to advanced oxydation phases (figure 4): a detailed analysis of these precipitates will be found elsewhere [20].

It is thus likely that diffusion of chemical species: Si and Fe, occurs inside the precipitates, and it can be assumed that several (Fe, Si) phases simultaneously co-exist, forming and vanishing in the same time in non-equilibrium conditions.

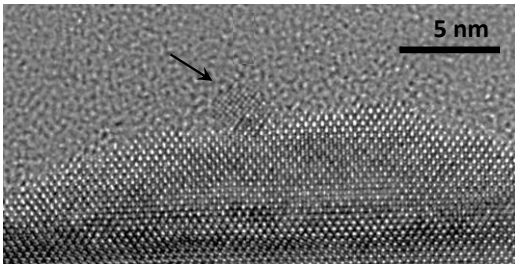

Figure 4 Nanometric FeSi precipitate at the top of a pyramid (oxidation conditions 1100°C, 12 min).

2.4 Diffusion, precipitation and dissolution of Fe at the moving SiO_2/Si interface The behaviour of implanted iron during the oxidation annealing may then be described as follows:

a) Diffusion towards the surface occurs in 10^{-2} s, when the sample is introduced in the furnace at 800°C ;

b) in less than 5 min at 900 °C, the main part of iron is precipitated as facetted $FeSi_2$ precipitates;

c) as the oxidation-front is moving forwards, precipitates follow the interface by Si oxidation–induced dissolution on one side, and simultaneous β-$FeSi_2$ growth on the other side;

d) β-$FeSi_2$ precipitates enriche in Fe because of preferential oxydation of Si atoms leading to the formation of Fe-rich phases for the longer times of oxidation;

e) nanometric Fe-rich clusters gettered in the SiO_2 oxyde layer remains observable in the vicinity of interfacial pyramids which would be the track of a dissolved precipitate overpassed by the oxidation front.

This easy-to-read storyline is hiding more complex behaviour: the dissolution/recrystallisation is an unavoidable mechanism to explain that precipitates are always located at the SiO_2/Si interface whatever the annealing time; nevertheless no change in precipitate compositions would be observed if it was not counterbalanced by the fast growth of the SiO_2 layer and the probable fast diffusion of iron within the β-$FeSi_2$ precipitates (and perhaps simultaneously in SiO_2).

As several of the steps described above are observed in single samples whatever the annealing time and temperature, we can reasonably conclude that competitive kinetics are involved resulting in the formation of the observed pyramidal defects: Fe segregation and precipitation, advance of the SiO_2/Si interface, Fe-silicide dissolution. The global SIMS measurements show that Fe is mainly located close to the interface; the local (TEM,APT) analyses reveal that the local increase of iron concentration results from unstable, dynamic mechanisms.

4 Conclusion Immediate segregation of Fe close to the surface, and fast re-crystallisation of the amorphous layer during the temperature increase from the room temperature up to 900 °C of the performed thermal annealing. No segregation of Fe is observed on extended defects like EOR; β-$FeSi_2$ precipitates were very frequently observed at the SiO_2/Si interface. The characteristics pyramidal defects reported in [10] were also observed by TEM.

The detailed analysis of the various oxidised samples strongly suggests that the formation of these defects at the SiO_2/Si interface is correlated with the presence of the precipitates. Moreover, a mechanism allowing understanding the formation of the pyramidal defects is proposed.

Competition between several kinetics (growth of silicon oxide, Fe-diffusion inside the precipitates, Fe-segregation at the moving interface, Fe-enrichment of precipitates, progressive dissolution of precipitates) is supposed to play a key role, leading to the observed complex microstructure : iron-silicides precipitates and associated pyramidals defects located at the moving SiO2/Si interface.

Acknowledgements The French Ministry of Industry has funded this work in the frame of the COMET project. (Industrial partners: ST Microelectronics, Lfoundry, Ion Beam Services, Rockwood, Biophy Research, TERA Environnement , VEGAtec)

References

[[1] G.D. Wilk, R.M. Wallace, J.M. Anthony, *J. Appl. Phys.* **89**, 5243 (2001).
[2] P.F. Schmidt and C.W. Pearce, *J. Electrochem. Soc.*, **128**, 3, 630 (1981).
[3] A.A. Istratov, H. Hielsmair and E.R. Weber, *Appl. Phys. A: Mat. Sci. Process.* **69**, 13 (1999).
[4] L.C. Kimerling and J.L. Benton, *Physica B* **116**, 297 (1983).
[5] K. Honda, T. Nakanishi, A. Ohsawa and N. Toyokura, *J. Appl. Phys*. **62**, 1960 (1987).
[6] Y. Kamiura, F. Hashimoto and M. Iwami, *Appl. Phys. Lett.* **53**, 1711 (1988).
[7] S. Sadamitsu, A. Sasaki, M. Hourai, S. Sumita and N. Fujino, *Jap. J. Appl. Phys.* **30**, 1591 (1991).
[8] D.J. Wong-Leung, J. Eaglesham, J. Sapjeta, D.C. Jacobson, J.M. Poate and J.S. Williams, *J. Appl. Phys.* **83**, 580 (1998).
[9] K. Oura, T. Kojima, F. Shoji and T. Hanawa, *Nucl. Instr. Meth. Phys. Res. B* **37-38**, 975 (1989).
[10] J. Bausells, G. Badenes and E. Lora-Tamayo, *Nucl. Instr. Meth. Phys. Res. B.* **55**, 666 (1991).
[11] J. F. Ziegler, *www.srim.org*
[12] A. Portavoce, N. Rodriguez, R. Daineche, C. Grosjean and C. Girardeaux , *Mater. Lett* **63**, 8, 676 (2009).
[13] M. Texier and J. Thibault-Pénisson, *Micron* **43**, 516 (2012).
[14] R.M. Drosd and J.Washburn, *J. Appl. Phys* **53**, 1, 397 (1982).
[15] C. Bonafos, D. Mathiot, A. Claverie, *J. Appl. Phys* **83**, 3008 (1998).
[16] E. Nes, *J. Appl. Phys* **42**, 3562 (1971).
[17] A.G. Cullis and L.E. Katz, *Phil. Mag.* **30**, 1419 (1974).
[18] W. Wijaranakula, *J. Appl. Phys.* **79**, 4450 (1996).
[19] A.A. Istratov, H. Hielsmair and E. Weber, *Appl. Phys. A: Mat. Sci. Process*. **70**, 489 (2000).
[20] A. De Luca, M.Texier, A.Portavoce, N. Burle, C. Grosjean, S.Morata, F. Michel, *J.Appl. Physics* **117**, 115302 (2015).